

## Article

# Depolymerization of Waste Plastic Using Bubble Column for Nano Alumina Blended Coating

Mohammed Alzuhairi \* , Hanaa Al-Kaisy and Mena Khedher

Department of Materials Engineering, University of Technology-Iraq, Baghdad 10069, Iraq; 130011@uotechnology.edu.iq (H.A.-K.); 130014@uotechnology.edu.iq (M.K.)

\* Correspondence: mohammed.a.alzuhairi@uotechnology.edu.iq; Tel.: +96-478-1171-0701

**Abstract:** In this study, we aimed to figure out how the depolymerization of polyethylene terephthalate produces monomers, dimers, trimers, and other oligomers of bis (2-hydroxyethyl) terephthalate. Polymerization was achieved in a bubble column reactor with 0.05 wt% 40–50 nm magnesium oxide nanoparticle as a catalyst. A bubble column reactor was used to perform the recycling process at the boiling point of ethylene glycol and atmospheric pressure. Depolymerized polyethylene terephthalate (DPET) was mixed with poly(methyl methacrylate) and reinforced with 1% Nano Al<sub>2</sub>O<sub>3</sub>. The nanoparticles acted as a composite coating in low carbon steel protection. Adhesion strength and mechanical and structural properties were investigated for the composite, and the average coating thickness was 28.39 μm. The results showed that the hardness and adhesion forces between the substrate and composite coating increased with an increase in the amounts of DPET and nano-Al<sub>2</sub>O<sub>3</sub> per polymer resin. On the other hand, the thermal conductivity of the composite coating decreased with the addition of DPET because of an increase in the end chain movement in the composite coating induced by the retardant and an increase in cross-linking force. Furthermore, the bubble column demonstrated outstanding heat and mass transfer phenomena that reduced the reaction time to just 40 min for complete depolymerization and also reduced energy consumption.



**Citation:** Alzuhairi, M.; Al-Kaisy, H.; Khedher, M. Depolymerization of Waste Plastic Using Bubble Column for Nano Alumina Blended Coating. *Fluids* **2022**, *7*, 127. <https://doi.org/10.3390/fluids7040127>

Academic Editor: Mehrdad Massoudi

Received: 18 December 2021

Accepted: 22 March 2022

Published: 28 March 2022

**Publisher's Note:** MDPI stays neutral with regard to jurisdictional claims in published maps and institutional affiliations.



**Copyright:** © 2022 by the authors. Licensee MDPI, Basel, Switzerland. This article is an open access article distributed under the terms and conditions of the Creative Commons Attribution (CC BY) license (<https://creativecommons.org/licenses/by/4.0/>).

**Keywords:** bubble column; depolymerization; polyethylene terephthalate; recycling; nanoceramic; coating

## 1. Introduction

The bubble column is a form of equipment that raises the contact area between reactants, resulting in increased heat and mass transfer [1–3]. The bubble column's transfer phenomena boost reaction rates and reduce reaction time significantly. These advantages save materials and energy and lower process costs [4]. Nanocatalysts can significantly reduce reaction time compared to homogenous and catalytic reactions [5,6].

The use of a polymeric coating prevents corrosion concerns by virtue of the coating materials' high adherence and the improvement of the corrosion resistance of metal alloys [7]. Furthermore, coating materials are dimensionally stable, scratch-resistant, and UV resistant and exhibit minimal curing shrinkage [8,9]. Dip composite coatings are the most widely used technique, especially for protecting the surface of a material to provide additional optimum or functional properties for industrial applications [10,11]. Polymer-ceramic coatings have gained popularity due to their simplicity of application, low cost, and good coating consistency. Polymer-ceramics also have a broad utilization spectrum, including environmental barrier coatings, thermal barrier coatings, and material protection [12–14].

Plastic materials are often not resolvable with microorganisms and lead to environmental pollution, so it is necessary for them to be recycled and reused. Depolymerization of PET flakes boosts the formulation rate of PET-based epoxy resin in paint, which improves the wet paint and dry film qualities of epoxy-based paints, including waste bottles [15]. The inclusion of waste PET in the blend enhances the characteristics of smart memory alloy (SMAs), enhances stiffness, and enhances resistance to permanent deformation (rutting) [16].

Recycling polymers provides practical products that minimize the use of fresh raw materials while also lowering energy consumption, air pollution (due to incineration), and water pollution (due to landfilling) [17]. Recycling is the third aspect in the Reduce, Reuse, and Recycle waste pyramid [18], and it is a significant element of contemporary waste minimization. Recycled materials have been employed in coatings, pigments, and adhesives because of their great film-forming capability, exceptional cohesion, high strength, and excellent dimensional durability [19]. However, their limited corrosion resistance restricts their use [20,21]. In addition, surface alteration techniques, such as surface passivation, electrochemical polishing, and polymer-derived ceramic coatings, often limit ion emission.

In this work, depolymerized PET (DPET) was produced by means of the bubble column technique to increase transfer phenomena and reduce reaction time. Functionalizing PET as DPET helps to develop poly(methyl methacrylate) (PMMA) composite and nanoceramic powder blends. A coating composite, consisting of PMMA, DPET powder, and 1% nano-alumina, was applied via dip-coating to reduced carbon steel substrates.

## 2. Materials and Methods

Waste plastic bottles, ethylene glycol (EG), polyethylene terephthalate (PET), magnesium oxide (50 nm, as a catalyst), and nano-aluminum oxide (80 nm) were the fundamental materials employed in this work in the preparation of specimens.

A 4:1 mixture of molar EG to PET with nano-MgO was fluidized (fully depolymerized) at 190 °C for forty minutes. Heating of the total condensation (reflux) in the bubble column and closed system was applied, as shown in Figure 1. The porous mesh was applied to a 3 mm plate with a tight pore distribution. For a column diameter of 0.08 m, a column height of 0.15 m (HD), and a superficial gas velocity (VG) of 0.04 m/s, there was excellent agreement between the CFD predictions and experimental profiles of hold-up and bubble velocity close to the wall. The primary goal of this study was to highlight the chemical depolymerization of PET using ethylene glycol, PET-catalyzed, and air, observing the glycolysis process in a bubble column via a three-phase technique, using a nanocatalyst, MgO with 0.1 wt%, for 100 g of PET. Nitrogen was preheated to 150 °C. In comparison to traditional methods, the depolymerization time could be reduced because of the improvement in heat and mass transfer obtained through the use of the bubble. A small amount of nano-MgO is sufficient to complete depolymerization. The second stage consisted of the isolation of residual ethylene glycol from the previously-described mixture. Subsequently, the product was left to cool at room temperature. Finally, the mixture was purified from the solid products by washing with boiled distilled water and mixing using a magnetic stirrer hot plate. This process assists in removing the remaining EG.

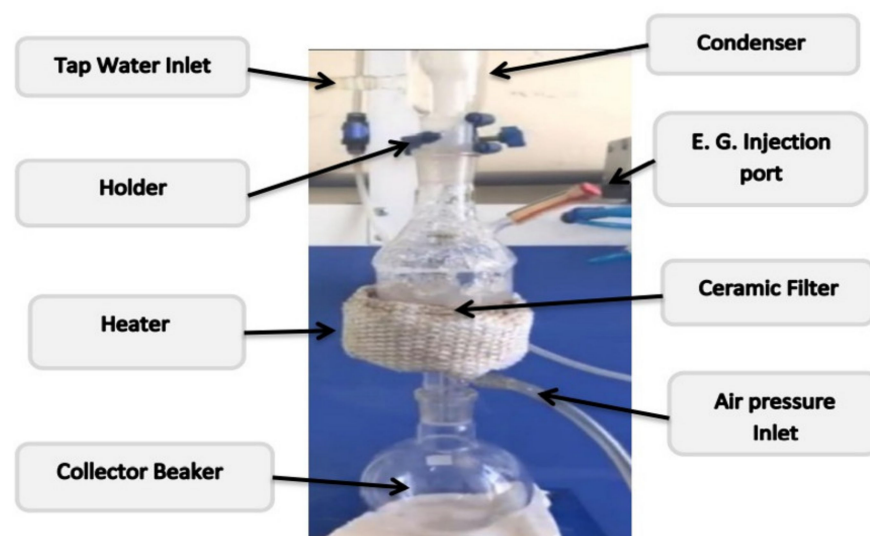


Figure 1. Preparing white crystalline DPET via the bubble column technique.

To generate white crystalline DPET chips, the mixture was cooled to ambient temperature and filtered under vacuum pressure. The mixture was then dried for 2 h at 60 °C to eliminate any moisture. The added percentages of the mix of DPET were 50%, 80%, 85%, 87%, and 90%. These amounts were added to 1 wt% nano- $\text{Al}_2\text{O}_3$ , and the remaining percentage was compensated for by PMMA. This composite was able to be applied via dip-coating onto a low-carbon steel substrate.

### 3. Results and Discussion

#### 3.1. Surface Roughness and Coating Thickness

A computerized optical microscope was used to measure the average coating thickness at a magnification of 40X. Figure 2 presents visual photographs of the composite coating, with an average coating thickness of 28.39  $\mu\text{m}$ .

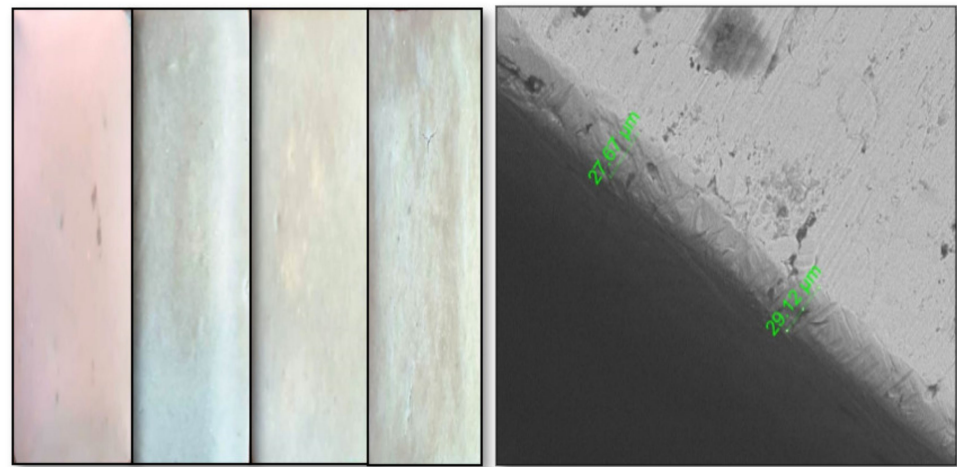


**Figure 2.** Optical photographs of the composite coating with DPET/PMMA-reinforced  $\text{Al}_2\text{O}_3$  nanoparticles on a low-carbon substrate, and the coating thickness.

With the addition of DPET powders, the surface of the films was roughened. The  $\text{Al}_2\text{O}_3$  nanoparticle content was responsible for enhancing the roughness of the coating for all samples, especially in the comparison between samples 4 and 5, as shown in Figure 3. The surface roughness increased when the DPET% increased.

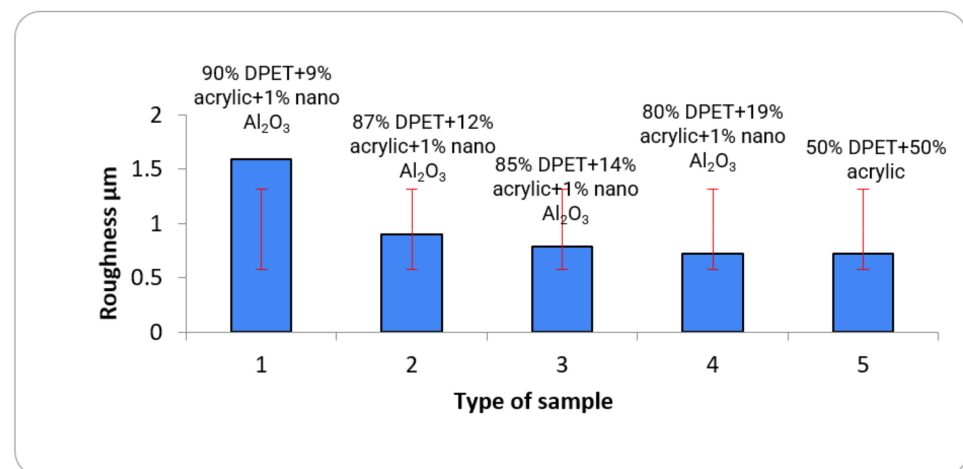


**Figure 3.** Surface roughness of the composite coating (DPET + PMMA with nano $\text{Al}_2\text{O}_3$ ).

#### 3.2. Blends Homogeneity Test

Figure 4 shows scanning electron microscopy (SEM) images of the surface of the pure coating specimen. The figure presents a micrograph of the cross-section view of the

dip-coating formed by the polymer coating. The morphology of the as-received polymer powder was used to produce dip coatings. The particles had an irregular and angular morphology, consistent with the mechanical crushing process, and created coating layers. The morphology was homogenous and without spherical cracks as the particles were able to tumble over each other and improve followability. The increase in DPET led to homogenous growth due to the reaction between the blended components through the functional group  $-OH$  in DPET. Figure 4b, with the highest DPET percentage, 90% DPET, showed better homogeneity, reflecting the blend's physical and mechanical properties, compared with the lower DPET blends shown in Figure 4a,c,d.

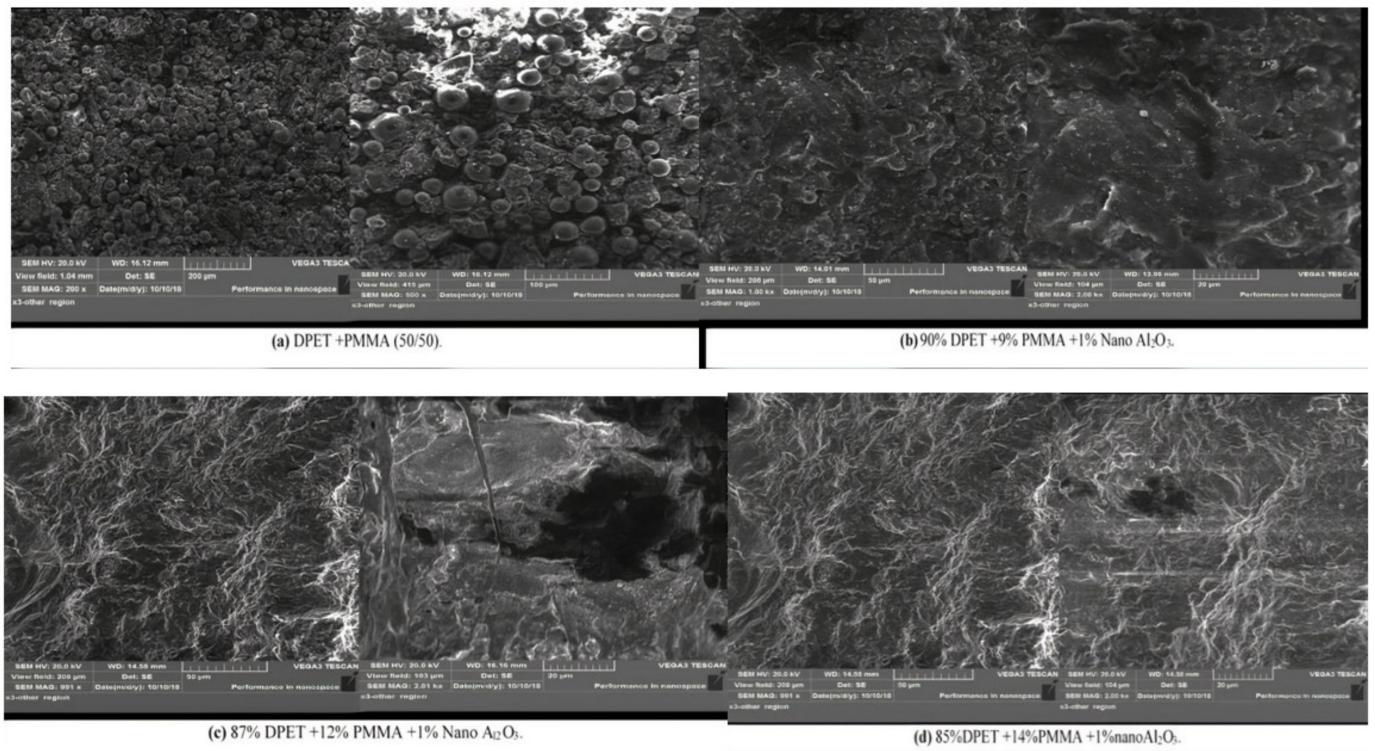


**Figure 4.** SEM micrograph of different blends' matrices.

### 3.3. Brinell Hardness

Figure 5 shows the Brinell hardness of the five coating samples. A significant increase in the hardness of the coating samples was observed with increasing DPET addition. The maximum hardness was observed in the composite coating, with a 40.1 HB (90%PET+1% nano-Al<sub>2</sub>O<sub>3</sub> coating and 28.88 HB for 80%PET+1% nano-Al<sub>2</sub>O<sub>3</sub>) increase in hardness compared with the as-received sample. It can be noted that the hardness of the DPET composite with Al<sub>2</sub>O<sub>3</sub> nanoparticles was dramatically enhanced. The homogeneous dispersion of the nanofillers was responsible for the observed hardness. The adequate bonding between the nanoparticles and the DPET matrix helps to resist indentation and leads to the formation of a two-phase system. The agglomerates and the polymer matrix act as hard and soft phases, resulting in non-uniform properties. The reaction between the DPET and other blend components leads to an increase in cohesion force, which is why the hardness improved.

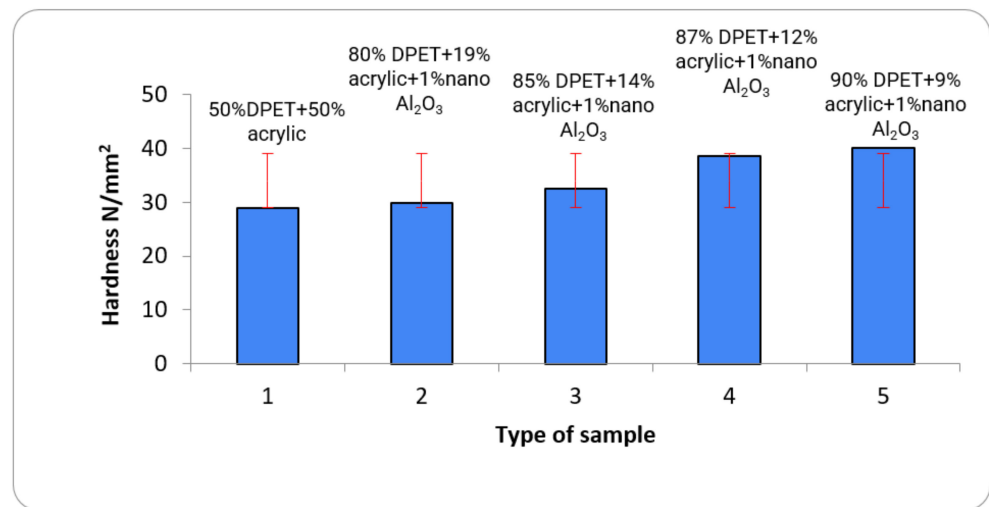


Figure 5. Effect of DPET addition on composite coating hardness.

### 3.4. Adhesion Strength Test

Figure 6 shows the adhesion strength for the coated samples at different concentrations of the composite coating (PET + nano-Al<sub>2</sub>O<sub>3</sub> and acrylic resin). For the five samples, a PMMA adhesive was utilized to attach the two coated parts. The adhesive sample was subjected to a 1 mm/min tension force until specimen failure was reached. The outcomes demonstrated that adding DPET raised the adhesive force between the substrate and the composite coating. The measurements in Figure 6 were merely designed to assess the strength of peeling of the PMMA and are not the real values for removing the hybrid coat from the substrate. Thus, peeling strength was substantially greater than the estimates, which could be attributed to good adhesion and interlocking with a surface between the coat and substrate with a considerable roughness prior to coating.

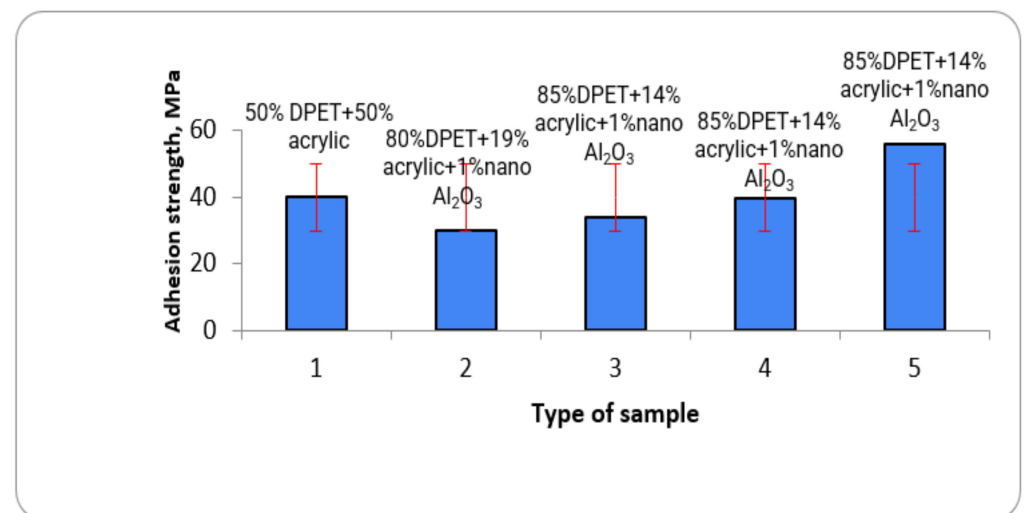


Figure 6. The adhesion coating composite strength of samples with DPET and PMMA.

Weakness in the homogenous variation between the blending material and DPET can be observed if we compare Figure 4a with Figure 4d for 50% DPET samples. However, in the case of the 90% DPET samples, the images showed good association based on the SEM images, and in consequence, this result was not very satisfactory, as in the rest of the DPET samples. Therefore, it can be concluded that the hardener material interacted well enough with the alternative commercial powder, based on the DPET ratios. However, the powder was commercially designed. Thus, the increase in adhesive strength can be attributed to the

powder's regular polymer distribution and the few hole and mass defects. This increase in adhesive strength is preferable in practical applications. Moreover, it is a good and cheap alternative that contributes to calculating the results of DPET.

Weak bonding between the blended materials—DPET and PMMA—was observed, as shown in Figure 6. This weak binding is evident in the bland homogeneity between the components in the 50% DPET. Compared with the 90% DPET samples, the images display a much better similarity between the mixture's components, indicating excellent cohesion among the principal elements. It can be said that the PMMA hardener reacted more efficiently or more effectively with the high proportions of the DPET powder, even though this hardener was commercially designed for PMMA. Thus, the DPET material can be a more effective commercial alternative due to its increased adhesion strength. This high adhesion strength can be attributed to the organized distribution of the powder with PMMA. The low number of defects (gaps or tangles) increases the adhesion strength, which gives more value to the coating, as shown in Figure 6. Despite the experience of the sample with the addition of 100% of DPET, it exhibited fragile cohesion. As a result, the minimal quantity of PMMA, which does not exceed 10%, ensures that the mixture performs well. The use of DPET improved the adhesion properties in coating applications, thus representing a low-cost alternative that could contribute to reducing waste problems worldwide.

### 3.5. Thermal Conductivity Test

As illustrated in Figure 7, the results showed the relation between the thermal conductivity of the composite coatings with different weight percentages of DPET, 1%  $\text{Al}_2\text{O}_3$  nanoparticles, and acrylic resin. When DPET and  $\text{Al}_2\text{O}_3$  nanoparticles were mixed with polymer resin, they operated as a cross-linking agent, causing DPET to bind to nanomolecules. This bonding decreased the free volume between acrylic molecules. As a result, the vibration of acrylic molecules was absorbed by the DPET [22], improving the thermal insulation of the coated layers. However, with the inclusion of DPET and nano- $\text{Al}_2\text{O}_3$ , this method caused additional difficulty in regard to the heat transfer in the composite coating, resulting in decreased thermal conductivity with the reduction of the percentage, due to the raising of the barrier of end-chain motion in the blended layer, raising the cross-linking force. In addition, DPET has a low thermal conductivity, which is why the thermal conductivity of the blends decreased when DPET% increased.

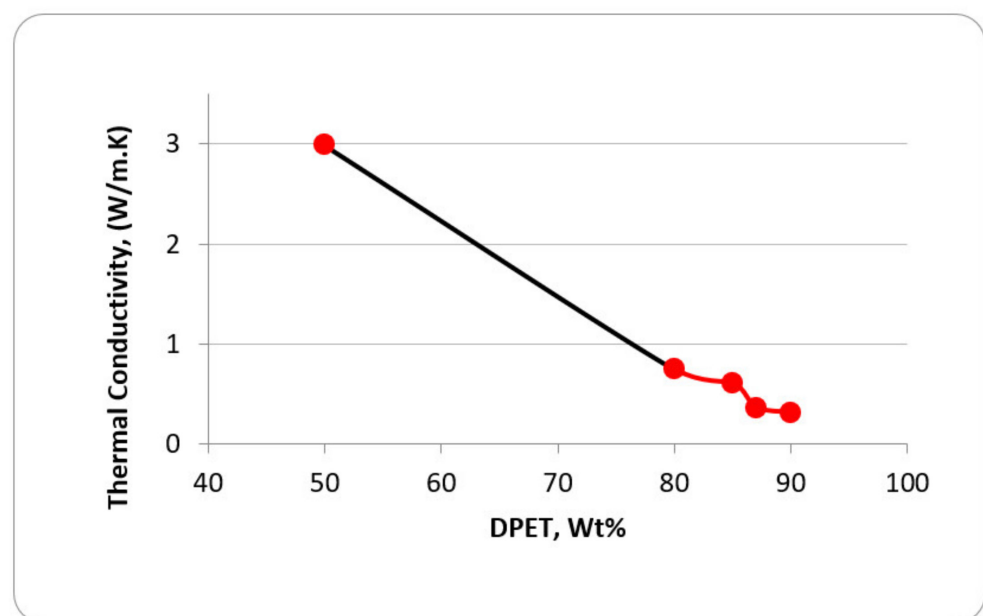


Figure 7. Thermal conductivity of composite coating with different percentages of DPET.

The optimum results achieved for mechanical properties, thermal conductivity, and surface roughness for each composite coating sample are summarized in Table 1. It can be concluded from the results shown in the table that the composites' coating properties increased with increasing the amount of DPET or waste plastic in the coating, despite (50%DPET + 50% acrylic) being more significant than that of the composite coating (DPET+ acrylic and 1% Nano- $\text{Al}_2\text{O}_3$ ) [23]. In any case, the waste plastic (DPET) tends to produce more adhesion characteristics in coating structures. Hence, they improve the thermal insulation, and more cohesion between the principal elements of coating produces excellent mechanical properties for composite coating.

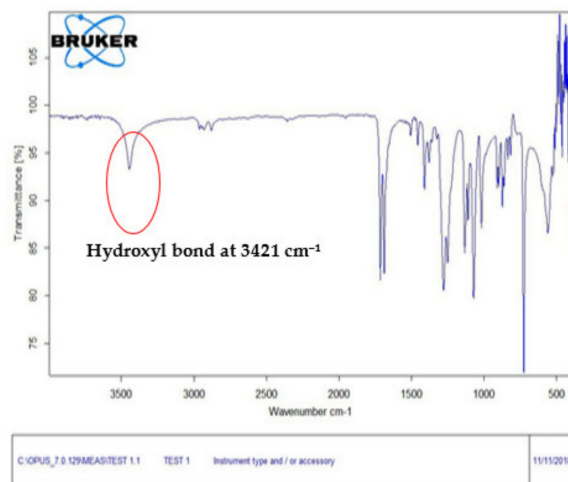
**Table 1.** The optimum mechanical and thermal properties.

#	Type of Coating	Adhesion Strength Mpa	HB N/m.m <sup>2</sup>	Surface Roughness $\mu\text{m}$	Thermal Conductivity (W/m.K)
1	90%DPET + 9% acrylic + 1% nano $\text{Al}_2\text{O}_3$	40.1	9.089	1.589	0.314
2	87%DPET + 12% acrylic + 1% nano $\text{Al}_2\text{O}_3$	38.6	7.847	0.905	0.366
3	85%DPET + 14% acrylic+1% nano $\text{Al}_2\text{O}_3$	32.6	7.03	0.786	0.611
4	80%DPET + 19% acrylic+1% nano $\text{Al}_2\text{O}_3$	29.9	5.88	0.724	0.748
5	50%DPET + 50% acrylic	28.88	4.12	0.72	2.99

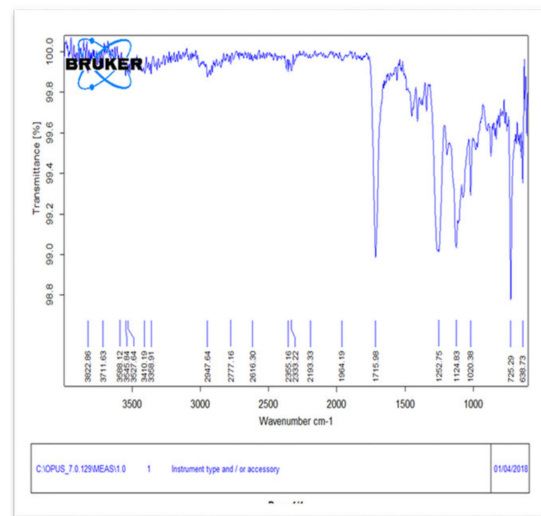
### 3.6. FTIR Characterization of DPET Blends

Aromatic (-C-H) wagging is visible at  $722\text{ cm}^{-1}$  in Figure 8a. The peak associated with aromatic (-C-H) out of the plane's winding was observed at  $872\text{ cm}^{-1}$ . At  $1094\text{ cm}^{-1}$ , asymmetric stretching of the (-O-C-C) was partitioned. Peaks were found at  $2961$  and  $2854\text{ cm}^{-1}$  (asymmetric stretching of -C-H),  $1504\text{ cm}^{-1}$  (stretching of aromatic C-C), and  $1454\text{ cm}^{-1}$  (stretching of aromatic C-C) (bending of C-H). Peaks attributable to (-C-H alkane) deformation were observed at  $1408\text{ cm}^{-1}$  and  $1371\text{ cm}^{-1}$ . The band of -OH at  $3421\text{ cm}^{-1}$ , the alkyl -CH band at  $2958\text{ cm}^{-1}$ , the C = O stretching band at  $1720\text{ cm}^{-1}$ , and the aryl group stretching band at  $1504\text{ cm}^{-1}$  were all visible in this figure; thus, the use of the bubble column reactor was an excellent technique for PET degradation [24].

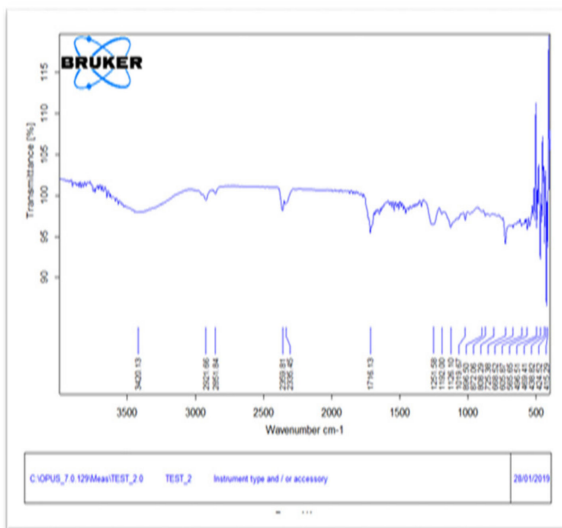
When comparing Figure 8a of pure DPET with Figure 8b–d it can be noted that the hydroxyl bond at  $3421\text{ cm}^{-1}$ , the functional group, in pure DPET disappeared in the other blends or composites, which indicates the occurrence of a chemical reaction between DPET and other materials. As a result of this reaction, the mechanical characteristics of the generated composite coatings improved, as did the cohesion strength and adhesion. Chemical recycling, involves polymer degradation to produce blends and additive materials for use in building and construction or for fuel production [25,26].



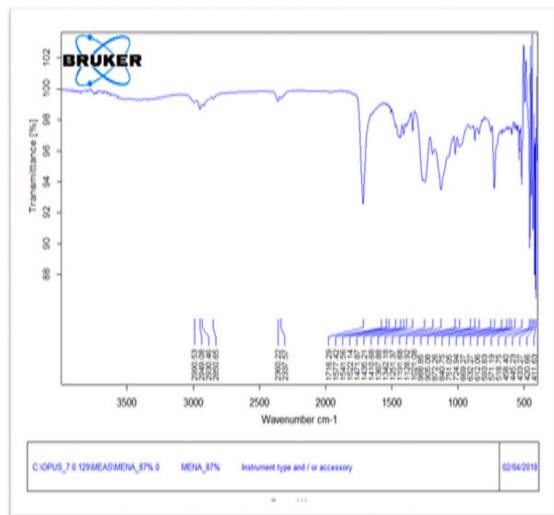
(a) Pure DPET.



(b) PMMA + DPET (50/50).



(c) 90%DPET +9%PMMA +1% Nano-Al<sub>2</sub>O<sub>3</sub>.



(d) 87%DPET +12%PMMA +1% Nano-Al<sub>2</sub>O<sub>3</sub>.

**Figure 8.** FTIR results of composite coatings with different percentages of (DPET + nano-Al<sub>2</sub>O<sub>3</sub> and PMMA).

#### 4. Conclusions

The use of a bubble column reactor was an outstanding approach for PET degradation with high heat and mass transfer and the most significant transfer phenomena, enabling users to shorten depolymerization time and thus save money. The average coating thickness was 1.6 μm. However, the measured thickness of the coating was not the same for all samples; this may have been due to the particle size of the DPET/nano-Al<sub>2</sub>O<sub>3</sub>/PMMA mixtures, and agglomeration could have occurred during species formation. The roughness of the surface decreased considerably for nano-powder contents, and the porosity also changed with the nano-powder content. After the adhesion test, composite coatings of DPET, Al<sub>2</sub>O<sub>3</sub> nanoparticles, and PMMA resin remained intact, representing the best adhesion characteristics. The results showed that the hardness and adhesion forces between the substrates and composite coatings increased with increasing the concentration of DPET or waste plastic. Because the thermal conductivity of the composite covering was reduced with the introduction of DPET, the composites might be employed in heat superinstallation. The retardant increased the motion of the terminal chains in the composite coating and the cross-linking force, resulting in a lowering of thermal conductivity. Research product

applications include coatings in military vehicles, construction equipment, ships, pipelines, pressure vessels, oil drilling platforms, and structural components.

**Author Contributions:** Conceptualization, M.A. and H.A.-K.; methodology, M.A.; software, M.A. and H.A.-K.; validation, M.K.; formal analysis, M.A.; investigation, H.A.-K. All authors have read and agreed to the published version of the manuscript.

**Funding:** This research received no external funding.

**Conflicts of Interest:** The authors declare no conflict of interest.

## References

1. Ogbonna, J.C.; Mashima, H.; Tanaka, H. Scale up of fuel ethanol production from sugar beet juice using loofa sponge immobilized bioreactor. *Bioresour. Technol.* **2001**, *76*, 1–8. [[CrossRef](#)]
2. Degaleesan, S.; Dudukovic, M.; Pan, Y. Experimental study of gas-induced liquid-flow structures in bubble columns. *AIChE J.* **2001**, *47*, 1913–1931. [[CrossRef](#)]
3. Forret, A.; Schweitzer, J.-M.; Gauthier, T.; Krishna, R.; Schweich, D. Influence of scale on the hydrodynamics of bubble column reactors: An experimental study in columns of 0.1, 0.4 and 1 m diameters. *Chem. Eng. Sci.* **2003**, *58*, 719–724. [[CrossRef](#)]
4. Alzuhairi, M. Bubble column and CFD simulation for chemical recycling of polyethylene terephthalate. *AIP Conf. Proc.* **2018**, *1968*, 030041.
5. Chiranjeevi, T.; Pragya, R.; Gupta, S.; Gokak, D.T.; Bhargava, S. Minimization of Waste Spent Catalyst in Refineries. *Procedia Environ. Sci.* **2016**, *35*, 610–617. [[CrossRef](#)]
6. Molnár, A.; Papp, A. Catalyst recycling—A survey of recent progress and current status. *Coord. Chem. Rev.* **2017**, *349*, 1–65. [[CrossRef](#)]
7. Majed, R.A.; Mahdi, M.; Al-Kaisy, H.A.; Maged, S.A.A. Corrosion Behavior for Al-Cu-Mg Alloy by Addition of SiO<sub>2</sub> Particles in Seawater. *Eng. Technol. J.* **2014**, *32*, 354–364.
8. Jiang, T.; Kuila, T.; Kim, N.H.; Ku, B.; Lee, J.H. Enhanced mechanical properties of silanized silica nanoparticle attached graphene oxide/epoxy composites. *Compos. Sci. Technol.* **2013**, *79*, 115–125. [[CrossRef](#)]
9. Chen, L.; Chenli, F.; Luo, Z.; Xin, Y. Study of Nano-Alumina Impact on the Performance of a CaCO<sub>3</sub>-Epoxy Composite Coating. *Nanomater. Nanotechnol.* **2016**, *6*, 39. [[CrossRef](#)]
10. Paul, D.R.; Robeson, L.M. Polymer nanotechnology: Nanocomposites. *Polymer* **2008**, *49*, 3187–3204. [[CrossRef](#)]
11. Petrović, Z.S.; Javni, I.; Waddon, A.; Bánhegyi, G. Structure and properties of polyurethane-silica nanocomposites. *J. Appl. Polym. Sci.* **2000**, *76*, 133–151. [[CrossRef](#)]
12. Chaudhari, L.; Nehete, K.; Sharma, R.; Bhattacharya, S.; Singal, V.; D’Melo, D. Study of erosion resistance and mechanical properties of unsaturated polyester based nano-composites. *IEEE Trans. Dielectr. Electr. Insul.* **2012**, *19*, 373–382.
13. Issa, R.A.; Al-Shroofy, M.N.; Al-Kaisy, H.A. Al<sub>2</sub>O<sub>3</sub>-TiO<sub>2</sub>-PMMA Bio-Composite Coating Via Electrostatic Spray Technique. *Eng. Technol. J.* **2021**, *39*, 504–511. [[CrossRef](#)]
14. Swain, S.; Sharma, R.A.; Bhattacharya, S.; Chaudhary, L. Effects of Nano-silica/Nano-alumina on Mechanical and Physical Properties of Polyurethane Composites and Coatings. *Trans. Electr. Electron. Mater.* **2013**, *14*, 1–8. [[CrossRef](#)]
15. Bal, K.; Ünlü, K.C.; Acar, I.; Güçlü, G. Epoxy-based paints from glycolysis products of postconsumer PET bottles: Synthesis, wet paint properties and film properties. *J. Coat. Technol. Res.* **2017**, *14*, 747–753. [[CrossRef](#)]
16. Ahmadinia, E.; Zargar, M.; Karim, M.; Abdelaziz, M.; Ahmadinia, E. Performance evaluation of utilization of waste Polyethylene Terephthalate (PET) in stone mastic asphalt. *Constr. Build. Mater.* **2012**, *36*, 984–989. [[CrossRef](#)]
17. Ferrari, K.; Gamberini, R.; Rimini, B. The Waste Hierarchy: A Strategic, Tactical and Operational Approach for Developing Countries. The Case Study of Mozambique. *Int. J. Sustain. Dev. Plan.* **2016**, *11*, 759–770. [[CrossRef](#)]
18. Acar, I.; Bal, A.; Güçlü, G. The use of intermediates obtained from aminoglycolysis of waste poly(ethylene terephthalate) (PET) for the synthesis of water-reducible alkyd resin. *Can. J. Chem.* **2012**, *91*, 357–363. [[CrossRef](#)]
19. Chen, D.; Huang, X.; Wang, P.; Liang, X.; Zhou, X. Recycling Effective Ways of Waste Plastics. *Eng. Plast. Appl.* **2012**, *40*, 92–94. [[CrossRef](#)]
20. Al-Zubaidi, A.B.; Al-Tabbakh, A.A.; Al-kaisy, H.A. Mechanical, Thermal and Wear Characteristics of Polymer Composite Material Reinforced with Calcium Carbonate Powder. *Eng. Technol. J.* **2014**, *32*, 519–532.
21. Safi, B.; Saidi, M.; Aboutaleb, D.; Maallem, M. The use of plastic waste as fine aggregate in the self-compacting mortars: Effect on physical and mechanical properties. *Constr. Build. Mater.* **2013**, *43*, 436–442. [[CrossRef](#)]
22. Al-kaisy, H.A.; Al-Gebory, L.; Mahadi, S.H. Preparation and Characterization of TiO<sub>2</sub>-ZrO<sub>2</sub> Coating Prepared by Sol-Gel Spin Method. *Iraqi J. Mech. Mater. Eng.* **2020**, *20*, 257–267.
23. Mohammed, A.S. UHMWPE Nanocomposite Coatings Reinforced with Alumina (Al<sub>2</sub>O<sub>3</sub>) Nanoparticles for Tribological Applications. *Coatings* **2018**, *8*, 280. [[CrossRef](#)]
24. Halla, M.; Alzuhairi, M.; Sarmad, I.I.; Saif, H.S. Ternary waste plastic blends for binding and adhesion. *Int. J. Environ. Stud.* **2021**. [[CrossRef](#)]

- 
25. Zahraa, H.A.; Zaidoon, S.M.; Alzuhairi, M.; Farooq, A.-S. Thermal and catalytic cracking of plastic waste: A review. *Int. J. Environ. Anal. Chem.* **2021**. [[CrossRef](#)]
  26. Zahraa, H.A.; Zaidoon, S.M.; Alzuhairi, M.; Farooq, A.-S. The yield of gasoline range hydrocarbons from plastic waste pyrolysis. *Energy Source Part A* **2022**, *44*, 718–731. [[CrossRef](#)]